ChemComm

Chemical Communications

Accepted Manuscript

Volume 54
Number 1
4 January 2018
Pages 1-112

ChemComm

Chemical Communications

rsc.li/chemcomm

ISSN 1359-7345

COMMUNICATION
S. J. Connon, M. O. Senge et al
Conformational control of nonplanar free base porphyrins:
towards bifunctional catalysts of tunable basicity

This is an Accepted Manuscript, which has been through the Royal Society of Chemistry peer review process and has been accepted for publication.

Accepted Manuscripts are published online shortly after acceptance, before technical editing, formatting and proof reading. Using this free service, authors can make their results available to the community, in citable form, before we publish the edited article. We will replace this Accepted Manuscript with the edited and formatted Advance Article as soon as it is available.

You can find more information about Accepted Manuscripts in the Information for Authors.

ROYAL SOCIETY
OF CHEMISTRY

rsc.li/chemcomm

COMMUNICATION

Solvent-Tunable Exciton-Charge Transfer Mixed State Enhances Emission of Functionalized Benzo[*rst*]pentaphene through Symmetry Breaking

Xiushang Xu,[a, #] Amy L. Vonder Haar,[b, #] Rengo Yoshioka,[a] Qizheng Zhang,[a] Serhii Vasylevskyi,[c] Andrew Musser*[b] and Akimitsu Narita*[a]

A benzo[*rst*]pentaphene (BPP) substituted by two bis(methoxyphenyl)amino (MeOPA) groups (BPP-MeOPA) was synthesized and clearly characterized by NMR and single-crystal X-ray analysis. Detailed investigations of its photophysical properties, including transient absorption spectroscopy analyses, revealed that the introduction of the MeOPA groups breaks the symmetry of the BPP core, improving its absorption and emission from an S_1 state with both excitonic and charge-transfer character.

Polycyclic aromatic hydrocarbons (PAHs) have been recognized as a promising building block for functional materials in photonics, optoelectronics, and spintronics due to their intriguing optoelectronic and magnetic properties.[1-4] A significant number of experimental and theoretical studies have demonstrated that the optical and electronic properties strongly depend on their size, shapes, and edge structures, such as armchair and zigzag.[5, 6] The optoelectronic properties of PAHs can be further modified by functionalizing the core, typically with electron-donating or -withdrawing groups.[7-10]

Benzo[*rst*]pentaphene (BPP), initially reported by Scholl and Neumann in 1922,[11] features a combination of zigzag and armchair edges, and can be a promising candidate for studying the effects of structural modification on the physicochemical properties toward different photonic applications. Nevertheless, despite the development of simplified synthetic methods for BPP,[12-16] its covalent functionalization with electron-donating/-withdrawing groups has been scarcely investigated. Recently, we reported that the relatively low

photoluminescence quantum yield (PLQY, 13%) of BPP was due to its symmetry-forbidden electronic transitions.[17] Interestingly, a dimer of BPP, 5,5'-bibenzo[*rst*]pentaphene (BBPP) displayed symmetry-breaking charge transfer between two BPP units and enhanced PLQY (44%). However, BBPP was still dominated by the same underlying electronic structure characterized by a low-lying dark state; the enhancement in PLQY arose principally from a reduction of the energy gap between bright and dark states, resulting in more efficient intensity borrowing.

In this work, we synthesized 2,11-di-*tert*-butyl-N^5,N^5,N^8,N^8-tetrakis(4-methoxyphenyl)benzo[*rst*]pentaphene-5,8-diamine (BPP-MeOPA **1**), functionalizing the BPP core with two bis(4-methoxyphenyl)amino (MeOPA) groups that have been widely used for preparing organic hole-transporting materials in views of their strong electron-donating ability.[18, 19] The photophysical properties of BPP-MeOPA **1** were investigated using transient absorption and photoluminescence spectroscopies in comparison with the parent BPP **7**, revealing the presence of solvent polarity-dependent intramolecular charge transfer and largely enhanced PLQY.

For the synthesis of **1** and **7**, 2-bromo-4-(*tert*-butyl)-1-iodobenzene (**3**) was initially prepared from the commercially available 2-bromo-4-(*tert*-butyl)aniline (**2**) by Sandmeyer reaction in 98% yield (Scheme 1). Then, **3** was subjected to the regioselective halogen–metal exchange reaction with isopropylmagnesium chloride at −78 °C, and reacted with dimethylformamide (DMF) to afford aldehyde **4** in 77% yield. Subsequently, dialdehyde **6** was obtained by Suzuki-Miyaura coupling of **4** and diboronic ester **5** in 85% yield. Di-*tert*-butyl-substituted BPP **7** was prepared by dehydrative π-extension (DPEX) reaction of **5** according to the literature procedure.[15] Next, **7** was brominated by *N*-bromosuccinimide (NBS) to give dibromo-BPP **8** in 94% yield. Finally, BPP-MeOPA **1** was obtained by Buchwald-Hartwig coupling of **8** and di-4-methoxyphenylamino (MeOPA) in 87% yield. The chemical structure of BPP-MeOPA **1** was unambiguously characterized by mass spectrometry, nuclear magnetic resonance (NMR), and X-

[a.] *Organic and Carbon Nanomaterials Unit, Okinawa Institute of Science and Technology Graduate University, 1919-1 Tancha, Onna-son, Kunigami-gun, Okinawa 904-0495, Japan, E-mail: akimitsu.narita@oist.jp*

[b.] *Department of Chemistry & Chemical Biology, Cornell University, Ithaca, NY 14850, USA, E-mail: ajm557@cornell.edu*

[c.] *Engineering Section, Research Support Division, Okinawa Institute of Science and Technology Graduate University, 1919-1 Tancha, Onna-son, Kunigami-gun, Okinawa 904-0495, Japan*

[#]These authors contributed equally to this work.
Electronic Supplementary Information (ESI) available: [details of any supplementary information available should be included here]. See DOI: 10.1039/x0xx00000x

COMMUNICATION

Journal Name

ray crystallography. Moreover, all proton NMR signals could be clearly assigned by ^1H–^1H correlation spectroscopy (COSY) and nuclear Overhauser enhancement spectroscopy (NOESY) techniques (Figures S11, 13-14, see ESI for further details).
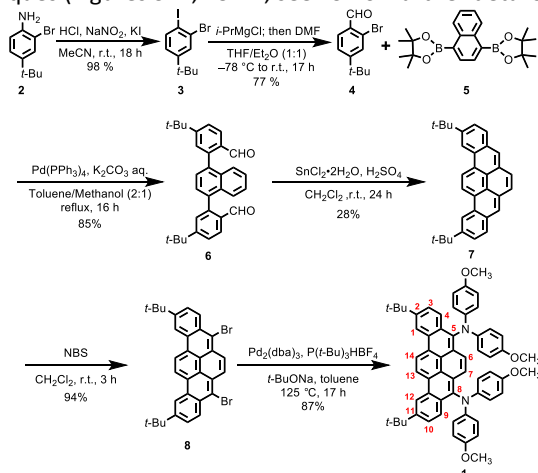
Scheme 1. The synthetic route to BPP-MeOPA **1** and BPP **7**.

The single crystal of BPP-MeOPA **1** was successfully grown from evaporation of CH_2Cl_2/CH_3OH solution, enabling its unambiguous structural determination by single-crystal X-ray analysis. As shown in Figure 1a, the single-crystal structure of **1** clearly revealed the BPP core and MeOPA substitutes at positions of C5 and C8 of BPP. The MeOPA was almost perpendicular to the BPP plane (dihedral angles 79°). In the crystal, along the *a*-axis, two BPP-MeOPA **1** are stacked almost parallel to each other. The plane-to-plane distance is 7.21 Å, indicating an absence of interactions between BPP-MeOPA **1** due to the existence of the *tert*-butyl and MeOPA groups at the peripheral position. Additionally, the X-ray structure is in good agreement with the one optimized by density functional theory (DFT) calculations.
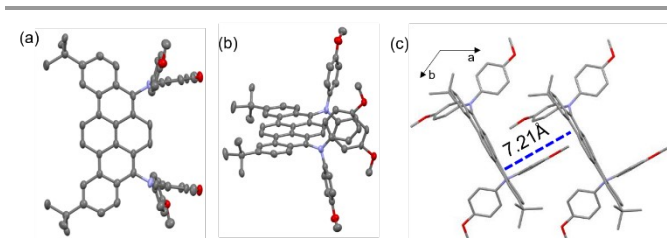

Figure 1. Single-crystal structure of **1**, (a) top view, (b) side view (thermal ellipsoids shown at 50% probability); (c) Packing arrangement of **1** in the crystal (solvents are omitted for clarity).

The UV-vis absorption spectra of **1** and **7** were measured in toluene solutions (Figure 2a). **1** and **7** display similar absorption peaks except for the low-energy absorption bands. The small peak located at 425 nm was observed for **7**, indicating the presence of the dark, symmetry-forbidden singlet state S_1, in agreement with our previous results.[17] The steady-state absorption of **1** suggests a comparable underlying electronic structure, but with noteworthy modifications. Most evidently, **1** displays a redshifted and broader low-energy absorption peak (502 nm) than that of **7**. The bathochromic shift of **1** reveals a reduced S_1 energy gap, which can be ascribed to the electron-donating property of the

MeOPA groups and the delocalization of frontier orbitals. Interestingly, this effect does not perturb the absorption of the principal BPP bright state, and we observe the same vibronic progression from 350-400 nm as in **7**. The lowest-energy band exhibits strikingly enhanced molar extinction coefficient in **1** (ε ~ 19000 M^{-1} cm^{-1}) compared to the S_1 state in **7** (ε ~ 1200 M^{-1} cm^{-1}), and at the same time there is clear reduction in the absorption of the S_2 state (ε ~ 70000 M^{-1} cm^{-1} in **7** versus ε ~ 32000 M^{-1} cm^{-1} in **1**). While some of the latter effect arises from increased broadening in **1**, integration across the band confirms a dimming of the S_2 transition. These effects are consistent with an enhancement of the intensity-borrowing mechanism previously[17] invoked to explain the absorption of S_1. We propose that part of this enhancement in **1** relative to **7** arises from symmetry breaking. The BPP core and MeOPA moieties interact electronically through charge-transfer coupling, which will be discussed in detail later in this paper, resulting in significant contributions to the wavefunction out of the BPP plane. This coupling is sensitive to the dihedral conformations around the amines. Such angles correspond to several low-frequency vibrational modes, resulting in significant geometric fluctuations at room temperature and accordingly a reduction in the symmetry. This effect yields significantly increased electronic disorder relative to **7**, broadening the vibronic progression observed in S_1 and S_2, and permits substantial brightening of the S_1 transition.
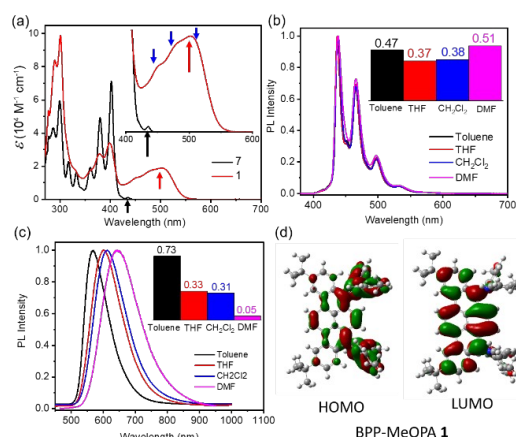

Figure 2. (a) Molar absorptivity of compounds **1** and **7** measured in toluene. Inset: the forbidden S_1 absorption peaks of **1** and **7** is indicated by arrows, approximate locations of vibronic structure marked with blue arrows. Normalized PL spectra of **7** (b) and **1** (c) were measured in toluene, tetrahydrofuran (THF), dichloromethane (CH_2Cl_2), and DMF. The absolute PL quantum yields (PLQY) in toluene, THF, CH_2Cl_2, and DMF are shown in the legend. (d) HOMO/LUMO distributions for BPP-MeOPA **1** were calculated using density functional theory (DFT) on the B3LYP/6-311G(d,p) energy level.

To gain further insight into the photophysical properties of **1** and **7**, their emission spectra were measured (Figure 2b-c). Both molecules exhibit mirror-image emission from their S_1 states with minimal Stokes shift, and the emission maximum in toluene red-shifted from 437 nm in **7** to 569 nm in **1**. Whereas **7** exhibits well-defined vibronic structure including 0→0, 0→1, 0→2 and 0→3 transitions, the PL of **1** is broad and featureless. The disappearance of the well-defined vibronic structure suggests a modified emission mechanism and is characteristic

Journal Name

COMMUNICATION

of intramolecular charge-transfer (ICT) states[21]. Indeed, **1** uniquely displays a considerable emission redshift and decrease in PLQY with increasing solvent polarity, a signature of ICT emission (Figure 2b-c). The formation of an ICT state in **1** upon photoexcitation is consistent with DFT calculations. We find that the highest occupied molecular orbital (HOMO) is principally localized on the MeOPA units, while the lowest unoccupied molecular orbital (LUMO) is located on the BPP core (Figure 2d). Time-dependent DFT calculations at M06-2X/6-311G(d,p) level indicate the lowest energy state contains major contributions from CT excitations, indicating partial electron transfer from MeOPA to BPP units (Figure S16, Table S1). Intriguingly, this effect appears to significantly enhance the luminescence of the molecule. The absolute PLQY of **1** in toluene was estimated to be 0.73, much higher than that of **7** (0.47). In principle, spatial separation of the electron and hole wavefunctions results in a reduction in the absorptivity and emissivity of a state (Figure S16), so the significant enhancement of these quantities in **1** is surprising.

To understand this unexpected behaviour, we turn to transient absorption (TA) spectroscopy. TA is a time-resolved technique capable of measuring fast, dynamic state evolutions induced in a molecule by photoexcitation. A pump pulse excites the sample and resonantly promotes electrons into higher energy states. A subsequent probe pulse then interrogates the formation, transformation, and decay of states generated by the pump at a range of delay times after excitation. Presented as the normalized change of probe transmittance $\Delta T/T$, the resulting TA spectra combine three primary features: the ground state bleach ($\Delta T/T > 0$), which monitors the total population of molecules removed from the ground electronic state; the stimulated emission ($\Delta T/T > 0$), which results from photon emission by electrons returning to ground state when triggered by the probe; and the photoinduced absorption ($\Delta T/T < 0$), which reflects absorption transitions of excited states to still higher levels. These processes involve absorption and/or emission of photons, but TA can also be used to resolve signatures of non-radiative decay via state lifetime determination. We performed TA on BPP-MeOPA **1** in five solvents that span a range of polarities: DMF, pyridine (Py), THF, chlorobenzene (CB), and toluene (Tol) at a concentration of ~20 µg mL^{-1} (Figures 3a, S19). We present here data for resonant excitation of the S_1 band at 490 nm. Within our temporal resolution (200 fs), we observe no change in the excited-state decay pathway following excitation at 400 nm directly into the S_2 state, with the only change a slight spectral broadening due to excess thermal energy (Figure S20).

All spectra show ground-state bleaching as a positive feature near 500-525 nm, in agreement with the red edge of the steady state absorption. Stimulated emission features are not distinguishable, likely indicating that the radiative transition does not have high brightness and is overpowered by the overlapping photoinduced absorption, the primary feature observed and spanning 525-825 nm. The initial state in the photoinduced absorption in all solvents exhibits fine structure with peaks ~660 nm, 710 nm, and 750 nm. On longer timescales we resolve a different spectral signature, with partial (toluene) or complete (all others) loss of this structure and the appearance of two distinct peaks. These then decay uniformly on an approximately nanosecond timescale. This stark change in spectral

shape indicates a change in electronic state and reveals that two excited states are required to explain the properties of **1**. Importantly, we observe systematic differences in this general pathway as a function of solvent polarity (Figure 3b). The final two-peak structure is most evident in highly polar DMF, while in toluene the spectral evolution is only partial, and we observe signs of the initial three-peaked structure throughout the measurement range. Moreover, the rate of this conversion tracks with solvent polarity: the initial state can barely be resolved in DMF and evolves within 500 fs, while the corresponding spectral evolution in toluene requires over 10 ps. The same can be said of the lifetime of the terminal state, which ranges from 2 ns in DMF to ~16 ns in toluene (Figure S28, Table S7).
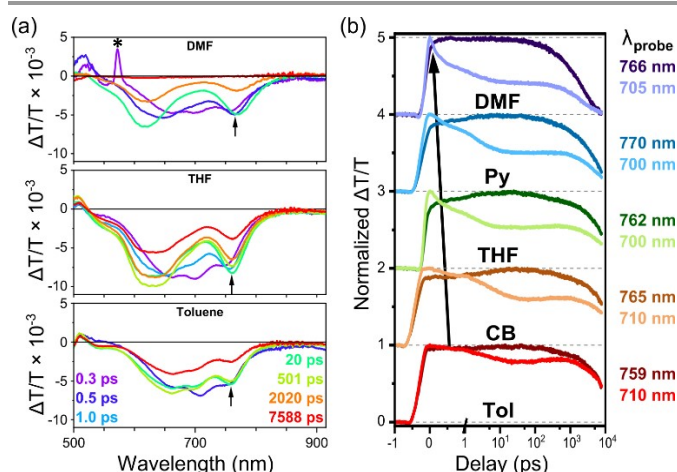

Figure 3. (a) TA spectra of **1** with 490 nm excitation in DMF, THF, and toluene. *denotes coherent artifact. Arrows highlight the position of the CT-related band shared by both states. (b) TA kinetic traces, including for pyridine and chlorobenzene, chosen to highlight the dynamics for the initial state (shorter λ) and final state (longer λ). Traces are offset for clarity. The arrow is to guide the eye along solvent dependence of crossover point.

We can identify the final state observed in TA through comparison with time-resolved photoluminescence (PL) spectroscopy experiments. We observe the same positive solvatochromism reported in Figure 2c, with no change in emission spectral shape during the measurement duration nor with change in excitation wavelength (confirmed using PL excitation mapping, Figure S23). As this ICT-like emission is stabilized with increasing solvent polarity, we see that the emission lifetime simultaneously decreases (Figure 4a). The lifetimes range from approximately 2 ns in DMF to 11 ns in THF to ~16 ns in toluene. As lifetime decreases, the PL quantum yield drops precipitously, becoming only 5% in DMF relative to 73% in toluene (Figure 2), suggesting a significant increase in nonradiative decay rate with stabilization. The slow PL decay dynamics closely follow the slow kinetics of the terminal state observed in TA (Figures S26 and S28), and we can thus assign the long-lived, two-peaked signature to a solvent-stabilized ICT state[21]. In a reference experiment, we electrochemically reduced **1** to generate the signature of BPP radical anions (Figure S24). The absorption of the reduced form agrees with the primary bands observed in TA, confirming the presence of BPP anionic character and thus an ICT state[22].
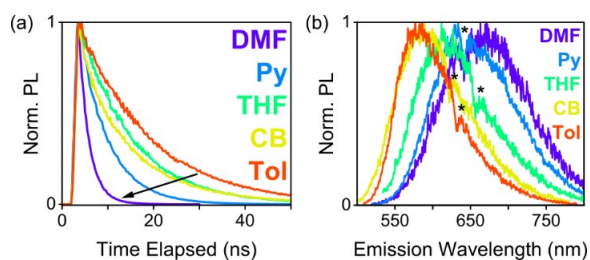
COMMUNICATION

Figure 4. (a) Solvent-dependent integrated PL dynamics of **1** following 490 nm excitation, and (b) corresponding normalized emission spectra. A systematic red shift and decrease in emission lifetime is observed with increasing polarity. * denotes a detector artifact.

This assignment suggests that the initial photoexcited state, S_1, is not itself an ICT state, as it exhibits different excited-state lineshape. Indeed, the presence of vibronic structure in the $S_0 \rightarrow S_1$ steady-state absorption (Figure S29) is typically characteristic of excitonic, rather than CT, species.[20,21] However, we note that the initial and ICT states share a common photoinduced absorption peak at approximately 750 nm (arrows in Figure 3a). Furthermore, careful analysis suggests that the 615 nm ICT state peak forms via a progressive blue shift from a 650 nm shoulder present in the initial state. Given this state is optically allowed with vibronic structure, shares spectral features with ICT, and can be induced to form an ICT state through interactions with the solvent, we propose that the initial S_1 state is a mixed state[20,21]. It has both excitonic and CT character, which can then relax into a weakly emitting, stabilized, pure ICT state through interaction with solvent dipoles[20,21]. In toluene, the solvent stabilization is relatively minor, resulting in only the slight enhancement of the CT character seen in TA, so the system remains in the bright mixed S_1 state.

This model highlights the delicate balance of factors governing the photophysics of **1**. Functionalization with MeOPA groups dynamically breaks the symmetry of this BPP derivative, allowing the S_1 state to become significantly brighter in absorption and emission. However, this effect comes at a cost: greatly increased susceptibility to form a stabilized ICT state with minimal orbital overlap and rapid nonradiative decay. Only in non-polar toluene are these competing factors balanced, to harness the advantages of symmetry-breaking functionalization without relaxation from the mixed S_1 state.

In summary, we have demonstrated the synthesis of donor-acceptor molecule BPP-MeOPA which was proved by X-ray crystallography. Photophysical properties of BPP-MeOPA were studied, which demonstrated intramolecular CT interactions and enhanced emission comparing with BPP. Interestingly, femtosecond TA spectroscopy in solutions of different polarity reveals that the S_1 state of BPP-MeOPA is mixed with both excitonic and CT character, which resulted in significantly brighter absorption and emission. This work demonstrates that there is great scope to enhance the optoelectronic properties of BPP chromophores and paves the way towards the development novel types of charge transfer in PAH derivatives to tune their optoelectronic properties and overcome their symmetry restrictions.

Notes and references

1. A. Narita, X. Y. Wang, X. L. Feng and K. Müllen, *Chem. Soc. Rev.*, 2015, **44**, 6616-6643.
2. X. S. Xu, K. Müllen and A. Narita, *Bull. Chem. Soc. Jpn.*, 2020, **93**, 490-506.
3. I. R. Márquez, S. Castro-Fernández, A. Millán and A. G. Campaña, *Chem. Commun.*, 2018, **54**, 6705-6718.
4. W. Chen, F. Yu, Q. Xu, G. Zhou and Q. Zhang, *Adv. Sci.*, 2020, **7**, 1903766.
5. Z. Y. Liu, S. Fu, X. M. Liu, A. Narita, P. Samori, M. Bonn and H. I. Wang, *Adv. Sci.*, 2022, **9**, 2106055.
6. X.-Y. Wang, X. Yao and K. Müllen, *Sci. China Chem.*, 2019, **62**, 1099-1144.
7. A. Keerthi, I. C.-Y. Hou, T. Marszalek, W. Pisula, M. Baumgarten and A. Narita, *Chem. Asian J.*, 2016, **11**, 2710-2714.
8. Y. Hu, L. F. Dössel, X.-Y. Wang, S. Mahesh, W. Pisula, S. De Feyter, X. Feng, K. Müllen and A. Narita, *ChemPlusChem*, 2017, **82**, 1030-1033.
9. Q. Chen, D. Wang, M. Baumgarten, D. Schollmeyer, K. Müllen and A. Narita, *Chem. Asian J.*, 2019, **14**, 1703–1707.
10. Y.-Z. Tan, B. Yang, K. Parvez, A. Narita, S. Osella, D. Beljonne, X. Feng and K. Müllen, *Nat. Commun.*, 2013, **4**, 2646.
11. H. N. R. Scholl, *Chem. Ber.*, 1922, **55**, 118-126.
12. E. Clar, *Ber. Deutsch. Chem. Ges.*, 1939, **72**, 1645-1649.
13. R. G. Harvey, J. Pataki, C. Cortez, P. Di Raddo and C. X. Yang, *J. Org. Chem.*, 1991, **56**, 1210-1217.
14. F.-J. Zhang, C. Cortez and R. G. Harvey, *J. Org. Chem.*, 2000, **65**, 3952-3960.
15. D. Lungerich, O. Papaianina, M. Feofanov, J. Liu, M. Devarajulu, S. I. Troyanov, S. Maier and K. Amsharov, *Nat. Commun.*, 2018, **9**, 4756.
16. X. Xu, A. Kinikar, M. D. Giovannantonio, P. Ruffieux, K. Müllen, R. Fasel and A. Narita, *Bull. Chem. Soc. Jpn.*, 2021, **94**, 997-999.
17. X. Xu, S. Gunasekaran, S. Renken, L. Ripani, D. Schollmeyer, W. Kim, M. Marcaccio, A. Musser and A. Narita, *Adv. Sci.*, 2022, **9**, 2200004.
18. P. Murugan, T. Hu, X. Hu and Y. Chen, *J. Mater. Chem. A*, 2022, **10**, 5044-5081.
19. Shahnawaz, S. Sudheendran Swayamprabha, M. R. Nagar, R. A. K. Yadav, S. Gull, D. K. Dubey and J.-H. Jou, *J Mater Chem C*, 2019, **7**, 7144-7158.
20. W. Li, Y. Pan, R. Xiao, Q. Peng, S. Zhang, D. Ma, F. Li, F. Shen, Y. Wang, B. Yang and Y. Ma, *Adv. Funct. Mater.*, 2014, **24**, 1609-1614.
21. A. M. Alvertis, S. Lukman, T. J. H. Hele, E. G. Fuemmeler, J. Feng, J. Wu, N. C. Greenham, A. W. Chin and A. J. Musser, *J. Am. Chem. Soc.*, 2019, **141**, 17558-17570.
22. S. Lukman, K. Chen, J. M. Hodgkiss, D. H. P. Turban, N. D. M. Hine, S. Dong, J. Wu, N. C. Greenham and A. J. Musser, *Nat. Commun.*, 2016, **7**, 1-13.